Compressive Stress-Strain Behavior of REBCO Coated Conductors and Cables

S. Xue, J. Kwon, Y. Guo, T. Garg, M. D. Sumption, and E. W. Collings

***Abstract*—Rare earth barium copper oxide (REBCO) coated conductor tapes and cables are promising material candidates for constructing high field magnets. In both the magnet constructing stage and operation stage, transverse pressure is exerted on the tapes/cables. Therefore, understanding the mechanical behavior of tapes/cable under transverse pressure and figuring out certain properties, such as modulus and stress limits, will be helpful for magnet design and magnet simulation study. We accomplished these goals by performing compression tests on several commonly used tapes/cables in high field magnets. We found that the mechanical behavior of tape stacks can be characterized in three distinct regimes. In the first regime (<20 MPa), tape stacks underwent flattening and self-relocation. Then in the second regime (20–60 MPa), the REBCO tape stack showed a modulus of 3.1 ± 7% GPa, and the Ni-plated REBCO tape stack showed a modulus of 1.7 ± 6% GPa. In the third regime (>60 MPa), the REBCO tape stack and its Ni-plated derivative had a modulus of 10 ± 11% GPa and 4.6 ± 9% GPa respectively. Roebel cable had similar mechanical behavior to the tape stack with three regimes, and the second and third regimes showed a modulus of 3.1 ± 5% GPa and 9.1 ± 11% GPa respectively. The conductor on round core (CORC) cable was more vulnerable to stress, and its fracture stress was around 27 MPa.**

***Index Terms*—Cables and current leads, HTS cables, mechanical properties, strain dependence, stress, strain measurement, superconducting tapes.**

I. Introduction

REBCO coated conductors are of interest for high field high energy physics (HEP) dipole and quadrupole steering and focusing magnet inserts, because of their exceptional high J_E at high field (>20 T). Many researches have demonstrated magnets made out of REBCO coated conductors tape, Roebel cables, and Conductor on Round Core (CORC) cables exhibit outstanding performance [1], [2], [3], [4], [5], [6], [7], [8]. For those coils, they were wound under tension. During the operation process, due to the Lorentz force, a transvers stress ranging from 100 MPa to 300 MPa will be exerted on the tape/cable surface [9], [10], [11].

For the non-insulation coil design, this transverse pressure can be utilized as a method to reduce the inter-tape/cable contact resistance (ICR) [12]. Under a transvers pressure that is greater than 100 MPa, the inter-strand contact efficiency, η ($\eta = ICR * contact\ area$), will be smaller than 50 $\mu\Omega$*cm^2 which can lead to good current sharing between tapes and therefore coils have better stability [13], [14].

On the other side, such a high stress level may lead to damage to the cables. For direct tape-to-tape contact, critical current degradation is limited to 2% under compression of 200 MPa, and less than 8% under compression of 550 MPa [15]. However, in the case of Roebel cable and CORC cable, due to the nature of the transposing tapes, their stress limits will tend to be closer to their shear stress (∼19 MPa) and cleavage stress (∼1 MPa) [16], [17], [18]. Therefore, the critical currents of Roebel cable and CORC cable are much more sensitive to pressure than tape stacks. The transverse pressure tolerance of critical current in Roebel cable is around 30-40 MPa [11], [15], [19]. Appreciable degradation of critical current in CORC cable starts at a pressure level of around 1.2 MPa, and as the diameter of the former decreases, the degradation of critical current due to transverse pressure becomes more severe [20], [21].

We have investigated the effect of transverse pressure on ICR of REBCO tape/cable in our previous studies [22], [23]. There are systematic studies about mechanical properties along tape/cable length and bending limits [24], [25], [26], [27], [28]. In this work, we focus on the mechanical behavior of REBCO coated conductor tape stacks and cables on the transvers direction. We performed compression tests on 4 types of samples, including 10-layer REBCO coated conductor tape stack, 10-layer Ni-plated REBCO coated conductor tape stack, Roebel cable, and CORC cable. The results concluded from this work can be applied to magnet design and as input parameters for magnet simulation.

II. Samples

In this work, four samples were tested, shown in Fig. 1. Sample 1 (24 mm * 4 mm * 1.3 mm) consists of 10 layers of commercially available SuperPower-SCS4050 2G HTS tapes (SP), and the specifications are given in Table I. Sample 2 (24 mm * 4.06 mm * 1.9 mm) is a ten-layer Ni-plated SP tape stack. Detailed Ni-plating process can be found in [23]. Sample 3 (15.8 mm * 11.8 mm * 1 mm) is a 9-layer Roebel

Manuscript received 13 November 2022; revised 28 January 2023 and 3 February 2023; accepted 5 February 2023. Date of publication 22 February 2023; date of current version 2 March 2023. This work was supported by the United States Department of Energy, Office of Science, Division of High Energy Physics under Grant DE SC0011721. *(Corresponding author: Shengchen Xue.)*

The authors are with the Center for Superconducting and Magnetic Materials, Department of Materials Science and Engineering, The Ohio State University, Columbus, OH 43210 USA (e-mail: xue.159@osu.edu).

Color versions of one or more figures in this article are available at https://doi.org/10.1109/TASC.2023.3247370.

Digital Object Identifier 10.1109/TASC.2023.3247370

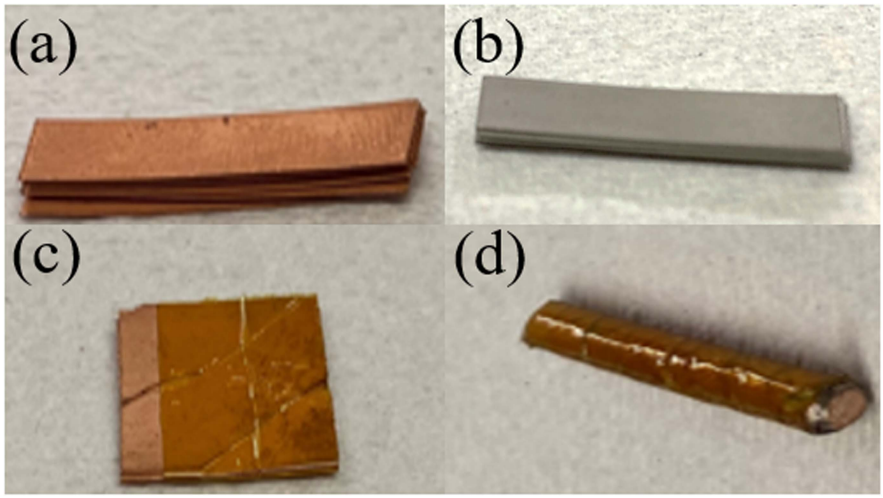

Fig. 1. (a) 10-layer REBCO tape stack, (b) 10-layer Ni-plated tape stack, (c) Roebel cable, (d) CORC cable.

TABLE I
SPECIFICATIONS OF THE REBCO COATED CONDUCTORS, SAMPLE 1

Component	Thickness (μm)
Cu stabilizer - YBCO side	20
Silver overlayer 1	2
REBCO	1
Buffer stack	0.2
Hastelloy	50
Silver overlayer 2	1.8
Cu stabilizer - substrate side	20
Tape thickness (mm)	~0.1
Stack Thickness (mm)	~ 1.3

TABLE II
SPECIFICATIONS OF ROEBEL CABLE, SAMPLE 3

Number of tapes in the cable	9
Tape width (mm)	5.6
Cable width (mm)	11.8
Pitch length (mm)	13
Cross-over angle (degree)	40
Inter-tape gap distance (mm)	0.4
Tape thickness (mm)	~0.1
Cable Thickness (mm)	~ 1

TABLE III
SPECIFICATIONS OF CORC CABLE, SAMPLE 4

Number of tapes in the cable	16
Cable diameter (mm)	3.4
Tape width (mm)	2
Tape thickness (mm)	0.045
Pitch length (mm)	6.22

cable that was fabricated by Karlsruhe Institute of Technology with SuperPower tape, and the cable specifications are listed in Table II. Sample 4 (24 mm in length) is a segment of a CORC cable provided by LBNL with ID 160823-Berkeley 250-C [29]. The CORC sample specifications are listed in Table III. For Sample 1 and 2 we performed five sets of tests on each. For Sample 3 and 4, we performed three sets of tests on each.

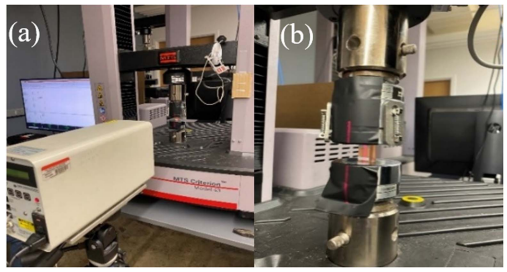

Fig. 2. (a) MTS model 43 testing frame, (b) error calibration of testing frame.

III. EXPERIMENTAL

A. Stress-Strain Test

We used MTS (model 43) for all compression tests. However, because all samples have thicknesses smaller than 3.5 mm, the systematic error from the testing frame is bigger than the thicknesses of the samples. Hence, it is necessary to subtract the error from the loading frame. We used 4 pieces of polycrystalline non-heat-treated copper blocks to perform error calibration. The dimensions of each copper block are 20 mm∗ 12 mm∗ 8 mm so that the surface area under compression is similar to those of Sample 1, 2 and 4. As shown in Fig. 2(b), the copper block was marked with two silver tapes, and a laser extensometer (model LE-01) was used to measure the displacement of the copper block. We applied pressure up to 200 MPa. Based on the value measured by the loading frame which contains the system error and the value measured by the laser extensometer which is the displacement of the sample, we were able to conclude an error correction function. Then we applied the error correction function to all the other measurements to calculate strains corresponding to stress levels. For Sample 1, 2, and 4 we applied stress up to 200 MPa. For Sample 3, it was tested up to 80 MPa. To make sure the samples were in contact with the testing frame, we used precision control to lower the pressing unit until we saw there was a small non-zero force exerted on

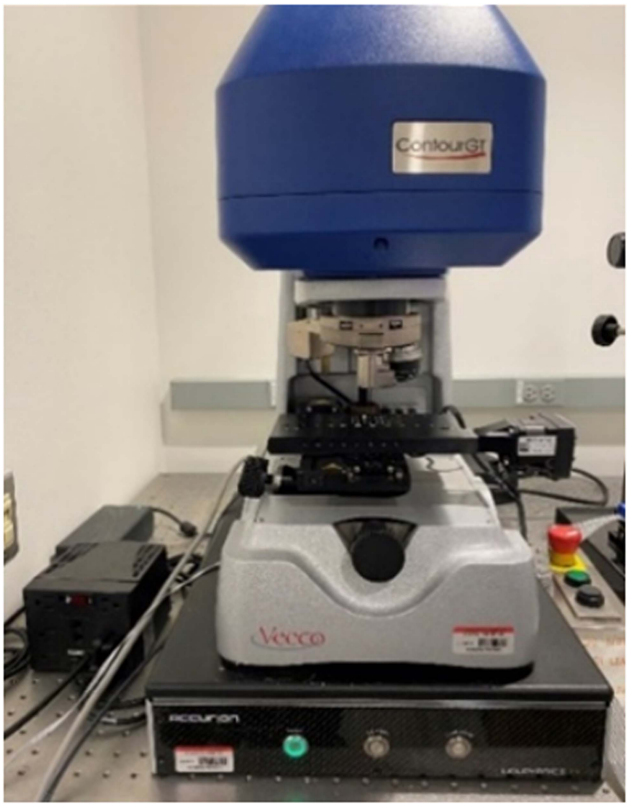

Fig. 3. Veeco model contour GT-K optical profilometer.

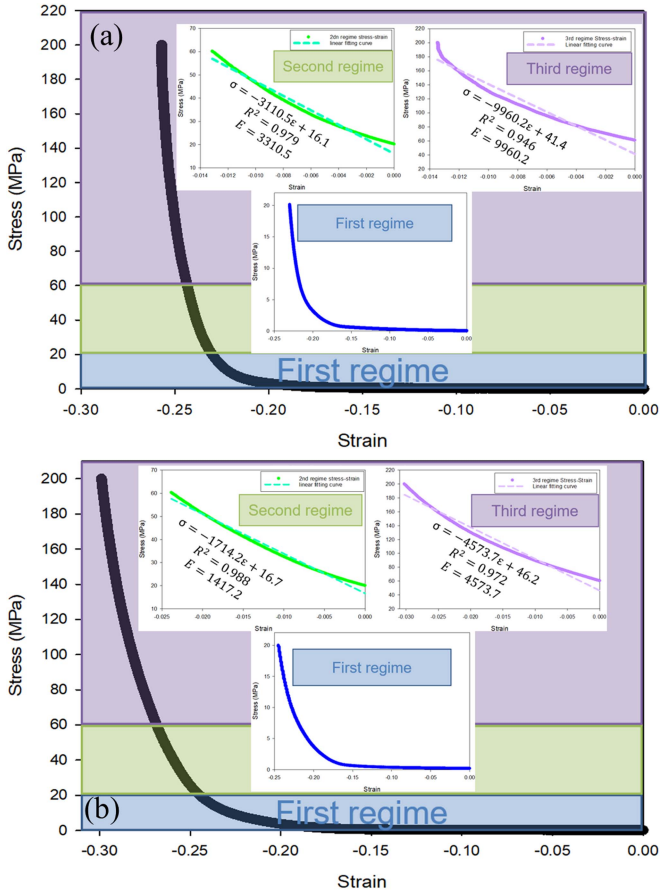

Fig. 4. Stress-strain curve of (a) Sample 1, (b) Sample 2. (Strain is determined as $\Delta L/L$.).

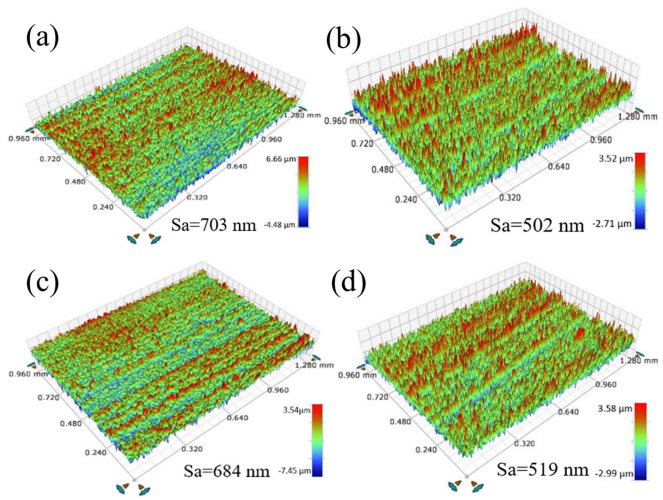

Fig. 5. Surface roughness of (a) Sample 1 before pressing, (b) Sample 1 after pressing, (c) Sample 2 before pressing, (d) Sample 2 after pressing.

the samples. Then we started measurements and applied a 0.003 mm/s strain rate for all samples.

The testing results for Sample 1, 2, and 3 were divided into three regimes based on pressure ranges. The pressure range and the fitting curve (1st order and 2nd order) of each regime were determined to produce the most consistent result (modulus) across the set of tests for a specific type of sample.

B. Surface Roughness Test

Surface roughness measurements were applied to Sample 1, 2, and 3 before and after the compression test by using the optical profilometer, shown in Fig. 3(Veeco, model Contour GT-K). The purpose of surface roughness measurement was to confirm that an appreciable amount of plastic deformation occurred during the compression test. For each sample, 8 measurements were taken to get better statistics. The roughness is presented as average roughness, SA, which can be interpreted as the deviation of a surface from its mean height.

IV. Results and Discussions

A. Compression Tests of Tape Stacks

The stress-strain behavior for Sample 1, the 10-layer SP tape stack, is presented in Fig. 4(a). The curve can be divided into three different regimes that are presented in the insets. Because the tapes contain curvature and their surfaces have certain roughness, as shown in Fig. 5(a), when 10 tapes are combined to form a tape stack, the thickness of the stack is about 30% more than the thickness of adding up 10 individual tapes. Therefore, in the first regime, where the pressure level was below 20 MPa and the strain was within 0.23, the displacement was mainly due to sample flatting, reducing the curvature, and tape self-relocation. For the second regime, where the pressure increased up to 60

MPa with 0.0135 additional strain, stress-strain behavior became mostly linear, and it showed a modulus of around 3.1 ± 7% GPa. The third regime of the stress-strain curve was a combination of elastic and plastic deformation. We fitted the third regime still linearly, because we thought that elastic deformation was more dominant, and the five sets of measurements showed an average modulus of 10 ± 11% GPa for the third regime

As shown in Fig. 4(b), Sample 2, the 10-layer Ni-plated SP tape stack, exhibited similar stress-strain behavior as Sample 1. The first regime was below 20 MPa, and the sample underwent 0.25 strain. The second regime was within the compression range from 20 MPa to 60 MPa, and it showed a modulus of 1.7 ± 6% GPa. The third regime which was above 60 MPa gave a modulus of 4.6 ± 9% GPa. In comparison with Sample 1, Sample 2 had lower modulus in both the second and third regimes, because Ni-plating introduced additional less stiff material relative to Hastelloy into the structure, and it is a typical trend for RE-BCO coated conductor tape that tape modulus decreases with increasing plating layer thickness.

The moduli extracted based on our measurement for both Sample 1 and 2 in the second and third regimes are low compared to the moduli of polycrystalline Cu and Ni which range from 100 GPa to 200 GPa. For both Sample 1 and 2, the second and third regimes contained certain plastic deformation and related work hardening. This could be a result due to the surface roughness of the tape, which could lead to a much higher local stress than the nominal stress value. More evidently, from Fig. 5, it can be seen that the average surface roughness of Sample 1 reduced from 703 nm to 502 nm (∼29% reduction), and the surface roughness of Sample 2 reduced from 684 nm to 519 nm (∼24% reduction). In addition, the amount of strain (>0.01) governed by the concluded modulus values were much larger than the technically specified strain limit (0.0002) for elastic modulus. In this case, it would be better to compare our results with the tangent moduli of materials that are commonly adopted to the classical bilinear isotropic hardening model which is used to perform FEM analyses on REBCO coated conductor tapes [30], [31], [32]. The tangent modulus of copper is 4 GPa. For sample 1, the modulus of the second regime (3.1 GPa) was close to the tangent modulus of copper. Then, as pressure increased, work hardening accumulated and Hastelloy, the stiffer component in the tape structure, became increasingly determinant to the stack modulus. For Sample 2, the stack modulus for both regime 2 and 3 were smaller due to increased plating thickness. The stack modulus increased from 1.7 GPa to 4.6 GPa, from a value that was lower than the tangent modulus of copper (4GPa) to a value that was similar. According to [33], the tangent modulus of electroplated Ni at 2% strain was ∼2.3 GPa [33], which was comparable to our measurement, 1.7 GPa. The intercept of the fitting line on the y-axis (pressure level) of each regime could be considered as the onset of a deformation regime given that the deformation regime was purely elastic. The fitting lines for the second regime of Sample 1 and 2 had intercepts (16.1 MPa and 16.7 MPa) that were fairly close to 20 MPa, but the third regime for both samples had intercepts (46.2 MPa and 41.4 MPa) different than the onset value, 60 MPa, for the third regime. Hence, that indicated there was more plastic deformation in the third regime than in the second regime. In both of the tape stack samples, the second regime was characterized by the tangent modulus of the softest material (copper in Sample 1, and nickel in Sample 2) in the structure. As the pressure level increased to the third regime, work hardening kept accumulating and the modulus of the harder materials, Hastelloy and copper, became representative of the samples. Because the moduli concluded from our measurement were controlled by the materials, the results should be applicable to tape stacks of different layers.

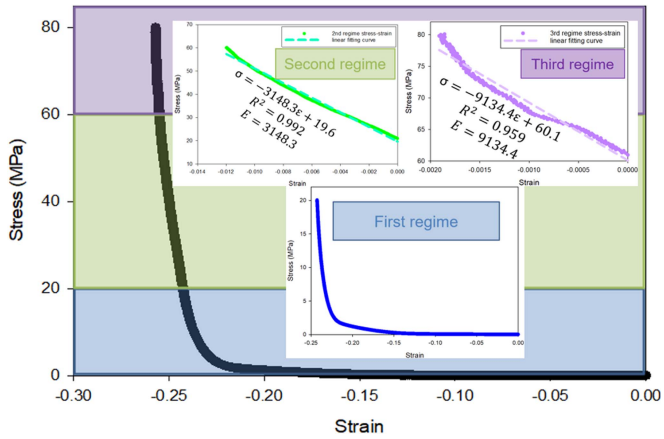

Fig. 6. Stress-strain curve of Sample 3. (Strain is determined as $\Delta L/L$.).

The results from our measurements follow the rule-of-mixture. However, the values of the modulus of nickel, copper, and Hastelloy need to be carefully considered. The as-received tape has a copper layer of 20 μm on each side, and the thickness of the Hastelloy is 50 μm. The Ni-plated tape has a nickel layer of 15 μm on each side. To apply the rule-of-mixture, we assume that the Hastelloy does not experience any plastic deformation, but the nickel and copper layer experience both elastic and plastic deformation. Therefore, we use tangent modulus for nickel and copper, 2.3 GPa [33] and 4 GPa [30] respectively, and use elastic modulus for Hastelloy, 190 GPa [30]. Given those, the calculated modulus is 8.8 GPa for Sample 1 and 5.2 GPa for Sample 2. Both calculated values are comparable to the measured moduli of the samples in their third regime.

B. *Compression Test of Roebel Cable*

Fig. 6 shows the stress-strain curve of the segment of Roebel cable. The first regime contained nearly 0.25 strain. Because the Roebel cable was fabricated with SuperPower tapes, the second regime and the third regime of the Roebel cable exhibited similar results as Sample 1, the 10-layer tape stack. The second regime of Roebel cable showed a modulus of 3.1 ± 5% GPa, and the third regime showed a modulus of 9.1 ± 11% GPa. However, it should be aware that unlike tapes or tape stacks which are resistant to pressure up to 550 MPa [15], the critical current of Roebel cable is very sensitive to compression, and even a compression of 30-40 MPa can lead to at least 20% of critical current reduction of the cable [11], [15], [19]. The reason for the high sensitivity of critical current to pressure was because of the

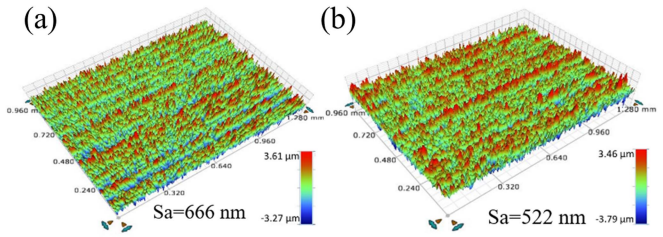

Fig. 7. Surface roughness of (a) Sample 3 before pressing, (b) Sample 3 after pressing.

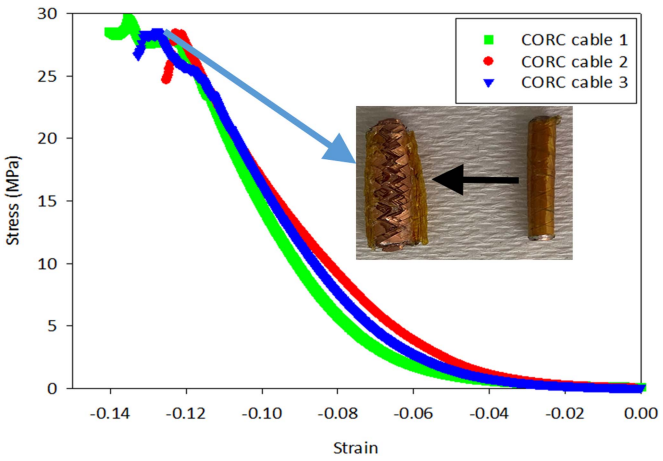

Fig. 8. Stress-strain curve of Sample 4.

low contact surface area between tapes in the Roebel cable [34]. One possible method to mitigate the critical current sensitivity to pressure is to apply epoxy impregnation.

Surface roughness measurement on the Roebel cable is presented in Fig. 7. The roughness measurements were performed on randomly selected areas on 8 of the 9 tapes in the cable. The average surface roughness of Sample 3 decreased from 666 nm to 522 nm (24% reduction), which is also comparable with Sample 1.

C. Compression Test of CORC Cable

The three compression tests on CORC cables showed consistent results, Fig. 8. The cables cracked at the pressure level of about 27 MPa. We calculated the transverse pressure applied on the CORC cables by normalizing the applied force to the product of sample length and cable diameter. If the same stress calculation is applied, based on other studies, the critical current of a CORC cable with a solid cylindrical copper former will start to decrease at stress as low as 1.2 MPa which is close to the cleavage stress limit of REBCO tape, and suffers at least 80% reduction when the transverse pressure reached 4.7 MPa [21], [22]. From the inset of Fig. 8, the damaged cable showed cleavage fracture surface. Hence if CORC cables are to be used for high field applications, external reinforcements, such as epoxy impregnation [11], [20] and stainless steel overbending covers, are necessary [6], [35].

V. Conclusion

In this study, we investigated the stress-strain behavior of four types of REBCO coated conductor tape/cables, including 10-layer REBCO coated conductor tape stack, 10-layer Ni-plated REBCO coated conductor tape stack, Roebel cable, and CORC cable. For samples in the form of tape stack, the stress-strain curve could be characterized into three different regimes. The first regime ended at a compression of 20 MPa, which is about the pre-stress applied during coil winding, such as a non-insulation coil. For the second regime (20-60 MPa), the 10-layer REBCO coated conductor tape stack showed a modulus of $3.1 \pm 7\%$ GPa, and the Ni-plated REBCO tape stack showed a modulus of $1.7 \pm 6\%$ GPa. For the third regime (>60 MPa), the REBCO tape stack and its Ni-plated derivative had moduli of $10 \pm 11\%$ GPa and $4.6 \pm 9\%$ GPa respectively. Roebel cable acted similarly to tape stack, which showed three different regimes with a modulus of $3.1 \pm 5\%$ GPa for the second regime and $9.1 \pm 11\%$ GPa for the third regime. CORC cable was the most vulnerable sample to transverse pressure, and it showed a fracture pressure of 27 MPa. These results can be used for magnet design and simulation, given the specific type of tape/cable used in the application and the transverse pressure level that is intended.

References

[1] A. C. Wulff, A. B. Abrahamsen, and A. R. Insinga, "Multifilamentary coated conductors for ultra-high magnetic field applications," *Supercond. Sci. Technol.*, vol. 34, Apr. 2021, Art. no. 053003.

[2] S. Hahn et al., "45.5-Tesla direct-current magnetic field generated with a high-temperature superconducting magnet," *Nature*, vol. 570, pp. 496–499, Jun. 2019.

[3] D. C. van der Laan, P. D. Noyes, G. E. Miller, H. W. Weijers, and G. P. Willering, "Characterization of a high-temperature superconducting conductor on round core cables in magnetic fields up to 20 T," *Supercond. Sci. Technol.*, vol. 26, no. 4, Feb. 2013, Art. no. 045005.

[4] R. Gupta et al., "Hybrid high-field cosine-theta accelerator magnet R&D with second-generation HTS," *IEEE Trans. Appl. Supercond.*, vol. 25, no. 3, Jun. 2015, Art. no. 4003704.

[5] H. W. Weijers et al., "Progress in the development and construction of a 32-T superconducting magnet," *IEEE Trans. Appl. Supercond.*, vol. 26, no. 4, Jun. 2016, Art. no. 4300807.

[6] D. C. Van Der Laan et al., "A CORC cable insert solenoid: The first high-temperature superconducting insert magnet tested at current exceeding 4 kA in 14 T background magnetic field," *Supercond. Sci. Technol.*, vol. 33, no. 5, Apr. 2020, Art. no. 05LT03.

[7] J. Fleiter, C. Lorin, and A. Ballarino, "On Roebel cable geometry for accelerator magnet," *Appl. Supercond.*, vol. 26, no. 3, Apr. 2016, Art. no. 4802805.

[8] J. Ruuskanen, A. Stenvall, V. Lahtinen, and E. Pardo, "Electromagnetic nonlinearities in Roebel-cable-based accelerator magnet prototype: Variational approach," *Supercond. Sci. Technol.*, vol. 30, no. 2, Dec. 2020, Art. no. 024008.

[9] J. Xia et al., "Stress and strain analysis of a REBCO high field coil based on the distribution of shielding current," *Supercond. Sci. Technol.*, vol. 32, no. 9, Jul. 2019, Art. no. 095005.

[10] X. Zhang et al., "Development of a 5 T class insert coil using YBCO coated conductors," *IEEE Trans. Appl. Supercond.*, vol. 29, no. 5, Aug. 2019, Art. no. 4601205.

[11] P. Gao et al., "Effect of resin impregnation on the transverse pressure dependence of the critical current in ReBCO Roebel cables," *Supercond. Sci. Technol.*, vol. 32, no. 5, Apr. 2019, Art. no. 055006.

[12] K. L. Kim et al., "Effect of winding tension on electrical behaviors of a no-insulation ReBCO pancake coil," *IEEE Trans. Appl. Supercond.*, vol. 24, no. 3, Jun. 2014, Art. no. 4600605.

[13] J. Lu, R. Goddard, K. Han, and S. Hahn, "Contact resistance between two REBCO tapes under load and load cycles," *Supercond. Sci. Technol.*, vol. 30, no. 4, Feb. 2017, Art. no. 045005.

[14] S. Xue, M. Majoros, M. D. Sumptio, T. Garg, and E. W. Collings, "FEM analysis of current sharing in REBCO coated conductor cables for particle accelerator applications," submitted for publication.
[15] D. Uglietti, R. Wesche, and P. Bruzzone, "Effect of transverse load on the critical current of a coated conductor Roebel cable," *Supercond. Sci. Technol.*, vol. 26, no. 7, May 2013, Art. no. 074002.
[16] Y. Yanagisawa et al., "Remarkable weakness against cleavage stress for YBCO-coated conductors and its effect on the YBCO coil performance," *Physica C*, vol. 471, no. 15-16, pp. 480–485, Aug. 2011.
[17] H. Maeda and Y. Yanagisawa, "Recent developments in high-temperature superconducting magnet technology," *IEEE Trans. Appl. Supercond.*, vol. 24, no. 3, Jun. 2014, Art. no. 4602412.
[18] S. Yin et al., "Degradation of REBECO coated conductors due to a combination of epoxy impregnation, thermal cycle, and quench: Characteristics and method of alleviation," *J. Appl. Phys.*, vol. 128, no. 17, Nov. 2020, Art. no. 173903.
[19] S. Otten et al., "Enhancement of the transverse stress tolerance of REBCO Roebel cable by epoxy impregnation," *Supercond. Sci. Technol.*, vol. 28, no. 6, Apr. 2015, Art. no. 065014.
[20] Y. Shi et al., "Analysis on the transverse compression performance of the CORC cable," *Supercond. Sci. Technol*, vol. 35, no. 12, Nov. 2022, Art. no. 125005.
[21] D. C. van der Laan, D. M. McRae, and J. D. Weiss, "Effect of the transverse compressive monotonic and cyclic loading on the performance of superconducting CORC cables and wires," *Supercond. Sci. Technol.*, vol. 32, no. 1, Nov. 2018, Art. no. 015002.
[22] S. Xue, M. D. Sumption, and E. W. Collings, "YBCO coated conductor interlayer electrical contact resistance measured from 77 K to 4 K under applied pressure up to 9.4 MPa," *IEEE Trans. Appl. Supercond.*, vol. 31, no. 5, Aug. 2021, Art. no. 7000305.
[23] S. Xue et al., "Electrical contact resistance in the REBCO stacks and cables with modified surface," *IEEE Trans. Appl. Supercond.*, vol. 32, no. 6, Sep. 2022, Art. no. 4802506.
[24] B. Christian, G. Mondonico, and C. Senatore, "Electro-mechanical properties of REBCO coated conductors from various industrial manufactures at 77 k, self-field and 4.2K, 19 T," *Supercond. Sci. Technol.*, vol. 28, no. 4, Feb. 2015, Art. no. 045011.
[25] S. Otten, A. Kario, A. Kling, and W. Goldacker, "Bending properties of different REBCO coated conductor tapes and Roebel cables at T = 77 K," *Supercond. Sci. Technol.*, vol. 29, no. 12, Oct. 2016, Art. no. 125003.
[26] D. C. van der Laan, "$YBa_2Cu_3O_{7-\delta}$ coated conductor cabling for low ac-loss and high-field magnet applications," *Supercond. Sci. Technol.*, vol. 22, no. 6, Apr. 2009, Art. no. 065013.
[27] D. C. van der Laan, X. F. Lu, and L. F. Goodrich, "Compact $GdBa_2Cu_3O_{7-\delta}$ coated conductor cables for electric power transmission and magnet applications," *Supercond. Sci. Technol.*, vol. 24, no. 4, Feb. 2011, Art. no. 042001.
[28] V. A. Anvar et al., "Bending of CORC cables and wires: Finite element parametric study and experimental valicdation," *Supercond. Sci. Technol.*, vol. 31, no. 11, Oct. 2018, Art. no. 115006.
[29] X. Wang et al., "A viable dipole magnet concept with REBCO CORC wires and further development needs for high-field magnet application," *Supercond. Sci. Technol.*, vol. 31, Mar. 2018, Art. no. 045007.
[30] N. C. Allen, L. Chiesa, and M. Takayasu, "Structural modeling of HTS tapes and cables," *Cryogenics*, vol. 80, no. 3, pp. 405–418, Dec. 2016.
[31] F. Pierro et al., "Finite-element analysis of the strain distribution due to bending in REBCO coated conductor for canted cosine theta dipole magnet application," *IEEE Trans. Appl. Supercond.*, vol. 29, no. 5, Aug. 2019, Art. no. 4600705.
[32] Z. Zhao, P. Moore, and L. Chiesa, "Structural finite element analysis of REBCO tape delamination with solid-shell element under various loads," *IOP Conf. Ser.: Mater. Sci. Eng.*, vol. 1241, no. 1, May 2022, Art. no. 012032.
[33] T. Nagoshi, T. M. Chang, S. Tatsuo, and M. Sone, "Mechanical properties of nickel fabricated by electroplating with supercritical CO_2 emulsion evaluated by micro-compression test using non-tapered mico-sized pillar," *Microelectron. Eng.*, vol. 110, pp. 270–273, Oct. 2013.
[34] J. Fleiter, A. Ballarino, L. Bottura, W. Goldacker, and A. Kario, "Characterization of Roebel cables for potential use in high-field magnets," *IEEE Trans. Appl. Supercond.*, vol. 25, no. 3, Jun. 2015, Art. no. 4802404.
[35] J. Stern et al., "Developing a vacuum pressure impregnation procedure for CORC wires," *IEEE Trans. Appl. Supercond.*, vol. 32, no. 6, Sep. 2022, Art. no. 4800904.